Influence of Titaniferous Phases on Tungsten Mineralizing Processes at the Giant Sisson Brook W-Mo Deposit, New Brunswick, Canada: Mineral-Chemical and Geochronological Assessment

Aaron L. Bustard [1,*] , **Wei Zhang** [2,*], **David R. Lentz** [1] and **Christopher R. M. McFarlane** [1]

[1] Department of Earth Sciences, University of New Brunswick, Fredericton, NB E3B 5A3, Canada; dlentz@unb.ca (D.R.L.); crmm@unb.ca (C.R.M.M.)
[2] Collaborative Innovation Center for Exploration of Strategic Mineral Resources, School of Earth Resources, China University of Geosciences, Wuhan 430074, China
* Correspondence: aaron.bustard@unb.ca (A.L.B.); zhangwei-china@live.cn (W.Z.)

Abstract: The Sisson Brook deposit is a low-grade, large-tonnage W-Mo deposit with notable Cu located in west-central New Brunswick, Canada, and is one of several W-Mo deposits in New Brunswick associated with fluids sourced from granitic plutons emplaced during the Devonian Acadian Orogeny. The younger Devonian-aged stockwork and replacement scheelite-wolframite-molybdenite (and chalcopyrite) mineralization straddles the faulted boundary between Cambro-Ordovician metasedimentary rocks with Ordovician felsic volcaniclastic rocks and the Middle Silurian Howard Peak Granodiorite, with dioritic and gabbroic phases. U-Pb dating of magmatic titanite in the host dioritic phase of the Howard Peak Granodiorite using LA ICP-MS resulted in a ^{204}Pb-corrected concordant age of 432.1 ± 1.9 Ma. Petrologic examination of selected mineralization combined with elemental mapping of vein selvages using micro-XRF and metasomatic titanite and ilmenite grains using LA ICP-MS indicates that saturation of titaniferous phases influenced the distribution of scheelite versus wolframite mineralization by altering the aFe/aCa ratio in mineralizing fluids. Ilmenite saturation in Ti-rich host rocks lowered the relative aFe/aCa and led to the formation of scheelite over wolframite. Altered magmatic titanite and hydrothermal titanite also show increased W and Mo concentrations due to interaction with and/or saturation from mineralizing fluids.

Keywords: W-Mo deposit; Sisson Brook; New Brunswick; scheelite; wolframite; titanite; ilmenite
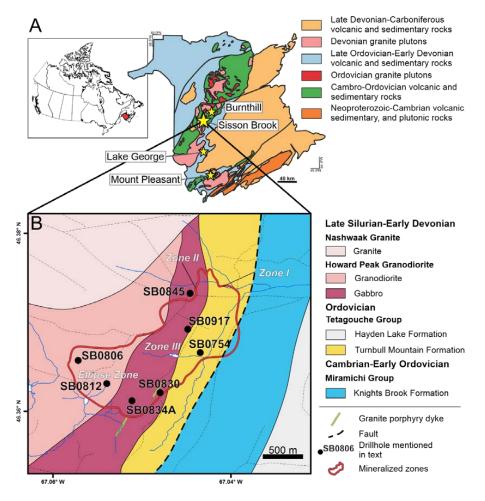
1. Introduction

Characterizing the interactions among mineral phases and ore-forming fluids is critical to understanding the mineral assemblages and mineralizing process occurring in a given deposit. The careful examination of petrographic relationships among minerals can assist in determining conditions required for their formation. The geochemistry of titaniferous minerals, such titanite ($CaTiSiO_5$), rutile (TiO_2), and ilmenite ($FeTiO_3$), can be indicative of W-Mo mineralization as these minerals can substitute W and Mo into their Ti site due to similar ionic radii [1]. Titanite can also accommodate REE, Y, U, Th, Pb, and Mn substitutions in its Ca site [1–3]; the examination of these substitutions can provide additional insight into the nature of fluid(s) responsible for the formation of a deposit (e.g., [1,3–5]). Titanite has been used extensively in the study of skarn deposits due to its abundance in calcium-rich host rocks, and it has been used as an indicator of fertility of source plutons for W-Mo mineralization [5] and for the identification of fluid sources [2]. Titanite is a common accessory mineral in intermediate metaluminous rocks [6], such as those hosting portions

of the Sisson Brook W-Mo deposit in eastern Canada [7], and its presence provides an opportunity to expand the understanding of how titanite and ilmenite record interactions with mineralizing fluids in porphyry-related systems. Furthermore, examination of compositional zoning in titaniferous phases can be used to elucidate successive influxes of mineralizing fluids and their evolution over time [8]. Uranium substitution allows titanite to be used as a geochronometer in both igneous and hydrothermal systems [2,6,9–11] allowing for a detailed study of deposit genesis from fluid sources to deposit formation.

New Brunswick is host to numerous Sn-W-Mo-Sb +/− Au deposits associated with Silurian to Devonian granitic plutons related to the Acadian Orogeny along the Ganderia–Avalonia boundary [12]. These deposits include Mount Pleasant (W-Mo) [13], Lake George (Sb and W-Mo-Au), Burnthill (W) [14], and Sisson Brook (W-Mo, [15–17], Figure 1 and Supplementary Figure S1). Sisson Brook, a low-grade, large-tonnage, porphyry-related W-Mo vein stockwork deposit situated in west-central New Brunswick [18,19], is the largest of these deposits [17], with mineral reserves of 387 Mt at 0.067% WO_3 and 0.021% Mo measured + indicated and 187 Mt at 0.050% WO_3 and 0.020% Mo inferred [20]. Detailed investigations of the Sisson Brook deposit include those of Nast [21], Nast and Williams-Jones [22], and Zhang [7] and Zhang et al. [19,23]. A limited discussion of the work presented here was initially described in Bustard et al. [24].

Figure 1. (**A**) General geology of New Brunswick (eastern Canada) with inset showing location of New Brunswick in Canada. Major Sn-W-Mo-Sb +/− Au deposits associated with Silurian to Devonian granitic plutons denoted by stars. Geology after Stewart et al. [17]. (**B**) Local geology of the Sisson Brook Deposit (outlined in red) with mineralized zones and collar locations of selected drill cores mentioned in text. Geology and mineralized zones modified from Rennie [20], which is modified after Fyffe et al. [25].

The deposition of scheelite and wolframite at the Sisson Brook deposit is due in part to the destabilization of KWO_4^- complexes resulting from the release of Fe and Ca during hydrothermal alteration of the host rocks [22]. Nast and Williams-Jones [22] recognized the relationship among host lithology and mineralization, but did not account for the role played by common titaniferous accessory minerals. Since the interaction of titanite and ilmenite affects the activities of both Fe and Ca, titaniferous phases can influence fluid composition, thereby favoring either scheelite or wolframite. This study aims to characterize the influence of titaniferous phases, i.e., titanite and ilmenite, on Fe and Ca in the mineralizing system and aFe/aCa effects on the distribution and degree of scheelite and wolframite mineralization.

2. Geological Setting

2.1. Geological Setting

The Sisson Brook deposit lies along the contact of Cambro-Ordovician volcanic and sedimentary rocks [20,25] that were intruded by Silurian to Devonian plutons ([26], Figure 1). The oldest rocks in the area are metamorphosed quartzite to shale of the Cambro-Ordovician Knights Brook Formation (Miramichi Group), which are conformably overlain by pyritiferous black shales interbedded with Ordovician felsic volcanic rocks of the Hayden Lake Formation (Tetagouche Group) [25]. To the west, the Knights Brook Formation is in contact with interbedded sandstone and tuff of the Ordovician Turnbull Mountain Formation (Tetagouche Group). Although not exposed, the contact of the Knights Brook and Turnbull Mountain formations is interpreted to be faulted, on the basis of quartz flooding and intense shearing near the contact [25]. These volcanic and sedimentary rocks were deposited at the margin of the Tetagouche-Exploits back-arc basin, an intracontinental back-arc that opened as a result of rifting behind the Popelogan arc in the Middle Ordovician. Closure of this back-arc occurred in the early Silurian during the Salinic orogenic cycle [27]. Later folding and faulting and early magmatism occurred during the Acadian Orogeny [20]. Regional metamorphism of volcano-sedimentary rocks was up to sub-greenshcist facies, and volcano-sedimentary rocks contain biotite, cordierite, andalusite, and garnet [21,22]. Andalusite-biotite-grade contact metamorphism occurs adjacent to the intruding Howard Peak Granodiorite and Nashwaak Granite, which comprise the major plutonic intrusive units in the Sisson Brook area [25].

The two major plutons underlie the Sisson Brook area, namely the Nashwaak Granite and the Howard Peak Granodiorite. The Howard Peak Granodiorite is highly foliated, medium grained, locally subporphyritic, and compositionally gradational between gabbro-diorite to granodiorite endmembers [25]. The granodiorite is composed primarily of plagioclase feldspar, 25–35 vol.% hornblende, and 5 vol.% quartz. This granodiorite also contains minor potassium feldspar, and accessory magnetite (locally hematized), titanite, apatite, and zircon. The gabbroic endmember resembles the granodiorite, but lacks quartz and contains minor pyroxene [20]. The eastern contact of the Howard Peak Granodiorite with the Turnbull Mountain Formation is highly sheared and contains xenoliths of country rock [25]. The intensely sheared nature of this contact likely provided an important conduit for the circulation of mineralizing fluids related to the formation of the Sisson Brook deposit [20,25]. Later, magmatism during late Acadian orogenesis is evidenced by biotite granite dykes, commonly cutting the Howard Peak Granodiorite, which intruded at 405.6 ± 2.5 Ma [19]. Partial biotitization to chloritization of the Howard Peak Granodiorite occurred as a result of contact metasomatism from the Nashwaak Granite [7].

The Nashwaak Granite is a medium-grained, equigranular to locally subporphyritic, massive, light grey to pink biotite granite. The Nashwaak Granite was emplaced between 419.2 ± 1.8 and 422.2 ± 1.7 Ma (U-Pb zircon concordia ages [19]), and is interpreted to be the product of partial melting of enriched sub-continental lithospheric mantle during slab breakoff during Salinic orogenesis [19,23].

Dykes and dykelets of porphyritic granite, originally thought to be related to the Nashwaak Granite, extend into the Howard Peak Granodiorite, indicating that the Nashwaak Granite was

emplaced later [20,25]. However, the latest intrusive phase identified are biotite granite porphyry dykes that are largely unaltered, crosscut mineralization [20], and dated at 364.5 ± 1.3 Ma (U-Pb zircon, [25]).

2.2. Mineralization

The Sisson Brook deposit occurs within a metallogenic belt that is associated with several other W occurrences, including the Burnthill (W), Lake George (Sb and W-Mo-Au), and Mount Pleasant (W-Mo) deposits [15]. Mineralization at the Sisson Brook deposit occurs in four zones: I, II, III, and the Ellipse zone (Figure 1B; [20]). Zones I and II are structurally controlled, tens of meters wide, and extend 100 s of meters along strike. Mineralization in zones I and II consists of scheelite and chalcopyrite with minor wolframite, and economically significant molybdenite mineralization is absent. Zone I is hosted by the Turnbull Mountain Formation, whereas zone II is hosted by the Howard Peak Granodiorite (both gabbroic and dioritic phases). Zone III, hosted mainly in the Turnbull Mountain Formation and partly in the Howard Peak Granodiorite, is located to the south of zones I and II and contains the bulk of the W and Mo mineralization at Sisson Brook. The Ellipse Zone is hosted in the Howard Peak Granodiorite (granodiorite and gabbro phases) [20]. Scheelite and molybdenite are the primary minerals of economic interest, whereas wolframite, where present, is commonly replaced by scheelite. Scheelite occurs throughout the deposit in mineralized quartz-sulphide veins, vein selvages, and in biotite alteration envelopes. Cogenetic molybdenite mineralization at Sisson Brook formed between 378.54 ± 1.71 and 376.45 ± 1.64 Ma as determined by Re-Os molybdenite model ages [7]. At Sisson Brook, the mineralizing fluids that deposited scheelite had relatively high fO$_2$ and low fS$_2$, at temperatures ranging from 330 °C to 430 °C at a pressure of approximately 500 bars (50 MPa) [22], whereas molybdenite deposition is associated with an increase in fS$_2$ [22].

3. Methods

3.1. Petrography

Standard polished thin sections prepared from drill core samples were examined using an optical petrographic microscope to ascertain relationships among the various ore and accessory mineral phases. A JEOL 6400 scanning electron microscope (SEM) equipped with an EDAX Energy Dispersive X-ray Analyzer (EDS) at the UNB Microscopy and Microanalysis Facility (MMF) (Fredericton, NB, Canada) was used to conduct a detailed follow up examination of samples using backscattered electron imaging (SEM-BSE). SEM-BSE imaging allows for the resolution of phases too small to be resolved optically and was used to identify zoning in titanite grains used for trace element mapping and dating. EDS analyses were used to confirm mineral phase identification. For select samples, corresponding polished slabs were also prepared for macro-scale examination.

3.2. Micro-XRF Mapping

The composition of polished thin sections was mapped using micro X-ray Fluorescence (micro-XRF) with a Bruker M4 Tornado instrument at the University of New Brunswick. Slides were scanned with a 20-μm spot and 35-μm spacing at 40 KeV and 500 mA with a 3-ms integration. Processing the XRF spectra collected during mapping allows for the calculation of desired elements that can then be presented as a compositional map. Compositional mapping of polished thin sections using micro-XRF, combined with other petrographic methods, allows for the comprehensive characterization of elemental distributions in a sample (e.g., [28,29]).

3.3. Image Analysis

Seven polished thin sections were imaged and analyzed as a preliminary study of the distribution and relationship between ilmenite-titanite and scheelite-wolframite. SEM-BSE images were captured using DPict software on the JEOL 6400 SEM at the UNB MMF, and were stitched together in Fiji image analysis software [30] using the grid/collection stitching function [31]. A series of images was captured

for each sample by manually moving the stage along a transect away from the mineralized vein with a 15% overlap between adjacent images. The image analysis relies on the fact that, in most cases, scheelite and ilmenite will have distinct grey levels in SEM-BSE images due to their relatively unique molecular masses. Two of the seven samples prepared were unsuitable due to interference of high mass minerals, i.e., galena and rare earth-rich phases, that were indistinguishable from scheelite in the images. After stitching, the greyscale SEM-BSE images were converted to binary black and white images using the threshold feature in Fiji to isolate the mineral of interest. A single erode routine followed by a dilate routine was applied to the image to remove small artifacts from the image (i.e., any particles smaller than 2 pixels), whereas all larger particles are returned to their original size with smoothed boundaries [32]. Scheelite and ilmenite particles were then counted using the analyze particles function in Fiji and the area of each grain calculated in μm^2. The WO_3 content of each sample was calculated using its empirical content in scheelite ($CaWO_4 - 80\%\ WO_3$) multiplied by surface area, resulting in a rough grade estimation of the 2D segment of the sample examined. Three portions of one sample, SB0812-12.8m, were measured to monitor data quality.

3.4. Mineral Element Mapping

Compositional mapping of minerals using laser ablation inductively coupled plasma-mass spectrometry (LA ICP-MS) can reveal heterogeneities and complex distributions of trace elements that are unresolvable with spot analyses [33,34]. Mineral maps of ilmenite and titanite were generated to examine the distribution of W and Mo in titaniferous minerals, and to assess the suitability of the titanite for U-Pb dating. A total of 11 grains were mapped using LA ICP-MS. Nine grains were analyzed from the Howard Peak Granodiorite, with five from the granodiorite/diorie and four from the gabbro phase), and two samples from tuff of the Turnbull Mountain Formation. Sampling concentrated mainly on the diorite and gabbro due to the greater abundance of large titanite grains in the coarser grained intrusive phases. Grains were selected to examine the relationship between ilmenite and titanite, and magmatic titanite was examined to determine zoning resulting from alteration during mineralization and variation imparted during growth. Elements measured with LA ICP-MS during mineral element mapping are ^{29}Si, ^{44}Ca, ^{45}Sc, ^{49}Ti, ^{51}V, ^{55}Mn, ^{56}Fe, ^{89}Y, ^{90}Zr, ^{95}Mo, ^{118}Sn, ^{140}Ce, ^{147}Sm, ^{153}Eu, ^{157}Gd, ^{172}Yb, ^{182}W, ^{232}Th, and ^{238}U.
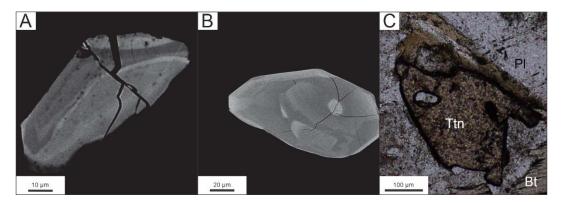
Element maps were generated by rastering a laser beam across the sample, thereby ionizing a small portion of the grain [33]. Both LA ICP-MS mapping and U-Pb geochronology were conducted at the University of New Brunswick's LA ICP-MS facility using a Resonetics M-50-LR 193ns laser coupled to an Agilent 7700x ICP-MS equipped with dual external pumps. The ablated aerosol is transferred to the ICP-MS in 4 mm OD Nylon™ tubing using a He carrier gas. A small amount of N_2 is added downstream of the ablation cell to enhance sensitivity and the Laurin Technic Pty 'Squid' smoothing device was removed for raster mapping to ensure fast washout times (5 orders of magnitude in 1 sec) to the ICP-MS. Prior to data collection, all laser ablation and ICP-MS parameters are tuned while rastering across NIST610 glass to achieve $^{248}ThO+/^{232}Th^+ < 0.2\%$, $^{44}Ca^{++}/^{44}Ca < 0.2\%$, and $^{238}U^+/^{232}Th^+ \sim 1.05$. Element maps were generated by rastering the laser across the sample using a 10-μm crater, a scan speed to 5 μm/s and a pulse rate of 10 Hz. Measurement of NIST612 glass, using the same raster conditions, was interspersed with the unknowns for external calibration and to correct for instrument drift. Periodic analyses of BCR-2G glass was used to check reproducibility (% relative deviation) that was better than 5% for heavy masses ($>^{87}Rb$) and 10–20% for light elements. Data reduction for compositional maps and U-Pb geochronology was carried out offline using Iolite v2.5 software (University of Melbourne, Melbourne, Australia) [35]. Compositional data were processed in a semi-quantitative way allowing the comparison elemental abundances across different minerals and using internal standardization to the (assumed) stoichiometric abundance of Ca in titanite. Standard procedures used for LA ICP-MS at UNB are outlined by McFarlane and Luo [36].

3.5. Whole Rock Geochemistry

Twenty samples were analyzed using Instrumental Neutron Activation Analysis (INAA) and Inductively Coupled Plasma-Mass Spectroscopy and Optical Emission Spectroscopy (ICP-MS, -OES) for geochemistry at Actlabs in Ancaster, ON, Canada. Two samples containing W in excess of the detection limit (10,000 ppm) were analyzed using ICP-MS following sodium peroxide fusion. Samples sent for geochemical analysis correspond with a subset of polished thin sections and slabs, and analysis was carried out to determine whether petrologic observations at the microscopic scale were mirrored in the macro-scale bulk geochemistry of the system. Data quality was monitored using CANMET standards GTS-2a (gold ore tailings from Timmins, ON, Canada) and BH-1 (wolframite ore from the Burnthill deposit, NB, Canada) from the Canada Centre for Energy and Mineral Technology (CANMET), and PR-1 (molybdenum ore from the Preissac Mo-mine near Cadillac, QC, Canada [37]).

3.6. U-Pb Dating

LA ICP-MS was used to date titanite from diorite of the Howard Peak Granodiorite. The U-Pb decay series was used to determine the age of titanite, as LA ICP-MS mineral element mapping of magmatic titanite indicated sufficient concentrations of U were present. Several of the titanite crystals investigated have U contents in excess of 100 ppm, considerably higher than the 10–100-ppm U range typical of titanite [9]. Preliminary attempts using zircon to date the granodiorite series were made since zircon is often the preferred mineral for U-Pb geochronology [38], but extensive dissolution–reprecipitation reactions [39,40] resulted in a spectrum of ages (see Figure 2A,B).

Figure 2. Images of zircon and titanite: (**A,B**) SEM-BSE images of zircon collected from diorite with gamma adjusted to highlight zoning (both grains from sample collected from drill core SB0806 at 69 m). (**C**) Transmitted light image of magmatic titanite grain used for geochronology (sample collected from drill core SB0806 at 63.7 m).

For titanite U-Pb geochronology, the laser was operated at 4 Hz, 4 J/cm^2 and with a 17-μm crater. Measurement of Khan Mine titanite, using reference isotope values from Heaman [41], was used as a primary isotope ratio standard with NIST610 used to calculate concentrations. For in situ U-Pb dating, the ICP-MS analyte dwell times (ms) are set to be approximately inversely proportional to expected ion beam size: ^{44}Ca (10), ^{202}Hg (10), ^{204}Pb (40), ^{206}Pb (30), ^{207}Pb (70), ^{208}Pb (10), ^{232}Th (10), ^{238}U(20). Measurement of ^{202}Hg is used to peak-strip excess ^{204}Hg from any net ^{204}(Pb + Hg) above background (negligible) and a value of 137.88 was used to calculate ^{235}U from the net ^{238}U ion beam. Long-term (>5 years) reproducibility of several titanite standards used in the UNB lab is ~1% (2σ). The U-Pb dataset was reduced using the VizualAge plugin for Iolite [42]. The integration period for individual ablations was assessed using a live Concordia showing ^{204}Pb-corrected and uncorrected data ellipses. All U-Pb plotting and age calculations was carried out using Isoplot 3.75 [43].

Thirty-one laser spot analyses were collected on titanite. Grains analyzed were selected based on textural evidence for minimal post crystallization modification and care was taken to ensure that the crater generated by the laser for sampling was not located on any cracks in the mineral, although

zoning is present in the titanite. Figure 2C depicts a magmatic titanite grain from SB0806-63.7 m used for U-Pb geochronology.
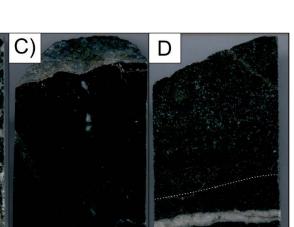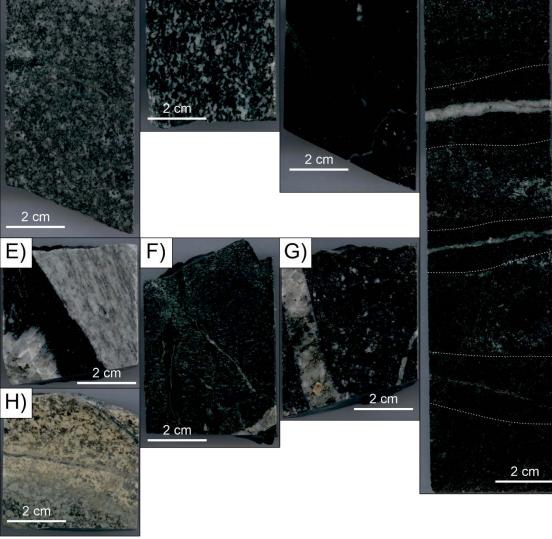
4. Results

4.1. Petrography

Of the polished thin sections examined, nine were collected from gabbro, three from diorite, and 23 from tuff or sedimentary rock. Pictures of select representative polished slabs are presented in Figure 3. The Howard Peak Granodiorite has a gabbroic phase that consists predominantly of medium-to coarse-grained plagioclase and hornblende. Plagioclase is almost completely sericitized (~60 vol.%), whereas the hornblende (~35 vol.%) is replaced by biotite and chlorite. Chloritic alteration is most common close to the mineralized veins and gives way to biotitization with increasing distance from the vein. Scheelite mineralization occurs as coarse grains in quartz veins and fine- to very fine-grained disseminated scheelite occurs in the country rocks immediately adjacent to veins. In contrast, molybdenite mineralization occurs only in the veins of the samples investigated. Pyrite occurs in all samples, whereas chalcopyrite occurs locally. Grains of ilmenite in solid solution with hematite, which are interpreted to be magmatic, as well as ilmenite with rims of titanite interpreted to be metasomatic (Figure 4A) were observed in some samples (<5 vol.%). Magmatic titanite is rare in gabbroic samples.

The diorite consists predominantly of plagioclase (~45 vol.%), biotite (~25 vol.%), hornblende (~15 vol.%), quartz (~15 vol.%). As in the gabbro samples, hornblende is altered to biotite further from the vein, and to chlorite in areas more proximal to the vein and within the vein selvage. The diorite samples contain metasomatic pyrite, chalcopyrite, ilmenite, and abundant (5 vol.%) medium-grained magmatic titanite. The ilmenite within the diorite is typically overgrown by metasomatic titanite. Apatite is also common in the diorite and locally occurs as rounded inclusions in titanite crystals. Plagioclase in the diorite samples is moderately to heavily sericitized. The mineralization present in the diorite consists of scheelite, with similar distribution as in the gabbro, with local pyrite and chalcopyrite. Disseminated sulfides generally do not extend more than 1 cm into the wall rock. Molybdenite was not observed in the altered diorite samples examined, although this may be the result of sampling bias. One diorite sample (collected from drill core SB0806 at 69 m) shows significant potassic alteration in the form of potassium feldspar up to 1 cm from a 0.5-cm quartz vein.

Plagioclase (50 vol.%) and amphibole (42 vol.%, mostly biotitized in mineralized samples) are the primary minerals in the mafic crystal tuff with accessory quartz (5 vol.%) and ilmenite (3 vol.%). The sedimentary rocks contain plagioclase (50 vol.%), which is commonly sericitized, and variable amounts of quartz (35 vol.%) and white mica (~15 vol.%). The felsic tuff is dominated by white mica and quartz. The white mica (muscovite) likely formed during regional deformation and possibly during subsequent contact metamorphism-metasomatism related to the intrusion of the Howard Peak Granodiorite. Accessory minerals in the sedimentary rocks include ilmenite (detrital and metasomatic), and titanite (detrital and metasomatic). The interpretation of whether grains were detrital or metasomatic was based on textural evidence of sedimentary transport (e.g., broken grains or rounded edges) for detrital grains and the occurrence as overgrowths and irregular boundaries for metasomatic minerals. Mineralization in the tuffs and sedimentary rock includes scheelite, wolframite, molybdenite, and chalcopyrite with pyrite and/or pyrrhotite. Fluorite is present in some veins. Rutile and detrital zircon grains are present in some sedimentary rocks. The sedimentary rocks are intensely sericitized (clastic plagioclase), as well as biotitized, and chloritized near mineralized veins. However, the degree of distinction between biotitization and chloritization appears to be less in the tuff and sedimentary rock than in the plutonic igneous rocks. Wolframite, where present in the studied samples, is always in contact with, proximal to, or replaced by scheelite, indicating that scheelite formed after wolframite in the tuff and tuffaceous sedimentary rocks (Figure 4B).
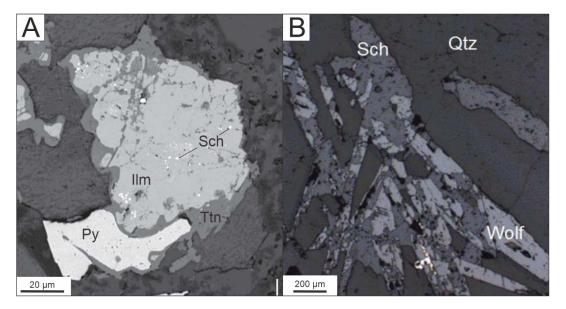
Figure 3. Images of representative polished slabs of rock types from the Sisson Brook Deposit. (**A**) Diorite, (**B**) gabbro, (**C**) argillite, (**D**) diabase dyke with visible alteration surrounding veins (selvage boundaries marked by white dashed line), (**E**) felsic augen tuff in contact with mafic tuff, (**F**) mafic tuff, (**G**) mafic crystal tuff, (**H**) sericitized gabbro showing altered selvage surrounding small carbonate and quartz veins.

In summary, the wallrock assemblages in mineralized zones at Sisson Brook show pervasive sericitic alteration of plagioclase, potassic alteration composed of biotite and potassium feldspar, which is then locally overprinted by chloritic alteration. Biotite alteration extends further from the veins than does chloritic alteration, and alteration by potassium feldspar is less common and is limited to within 1 cm of veins.

Mineralization of economic interest at Sisson Brook is locally dominated by scheelite and molybdenite. Empirically, most of the scheelite occurs as coarse grains in quartz veins or as fine grains in the selvage, whereas molybdenite occurs exclusively in veins. Examination of the diorite with SEM-BSE imaging identified the presence of scheelite inclusions within ilmenite and the flanking of ilmenite with titanite (Figure 4A). The relationship between scheelite and ilmenite is relatively

uncommon, but this relationship among titanite, ilmenite, and scheelite is not exclusive to the igneous rocks studied.
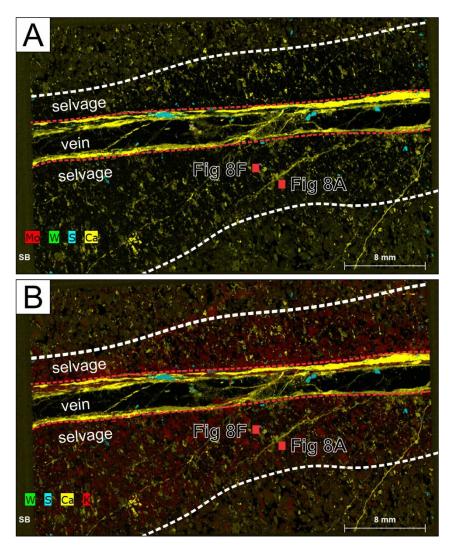

Figure 4. Mineralization at the Sisson Brook deposit. (**A**) SEM-BSE image showing μm scale scheelite (Sch) inclusions in metasomatic ilmenite (Ilm), which is rimmed by titanite (Ttn). Host rocks are dominated by quartz and biotite. Anhedral pyrite (Py) is also rimmed with titanite. Sample from drill core SB0806 at 69 m. (**B**) Relationship of scheelite (Sch) and wolframite (Wolf), with scheelite replacing blades of wolframite in a quartz (Qtz) vein in tuff. Sample from drill core SB0917 at 29 m.

4.2. Micro-XRF Mapping

Compositional distributions for sample SB0806-69 m were mapped using micro-XRF to determine the geochemical patterns of alteration resulting from mineralizing processes. Compositional maps for of Mo, W, S, and Ca are presented in Figure 5A and W, S, Ca, and K in Figure 5B. The elemental distributions are consistent with potassic alteration of calcium-bearing phases in the vein selvage, as there is a marked decrease in Ca near the vein and a corresponding increase in K. Calcium liberated by the potassic alteration is consumed to form scheelite from W complexes in solution and metasomatic titanite. Tungsten and Mo distributions are difficult to map given that they are primarily concentrated in discrete mineral grains, such as molybdenite (absent in this sample) or scheelite (green, mainly vein hosted). Tungsten contained in accessory minerals, such as titanite, is unresolvable in the maps due to its relatively low abundance.

4.3. Grain Size Analysis

Five of the seven samples investigated produced results suitable for image analysis, as ilmenite could not be measured in all samples due to locally low abundances. Aggregate data are presented in Table 1 and Figure 6. This preliminary measurement of grain size distribution indicates that scheelite grains outnumber ilmenite in mineralized intervals as ilmenite constitutes no more than 17% of the area occupied by scheelite (Table 1). Scheelite populations are also invariably skewed towards smaller grain size, although large grains account for most of the volume of mineralization (Figure 7).

Figure 5. Micro-XRF compositional maps for sample from drill core SB0806 at 69 m showing distribution of (**A**) Mo, W, S, and Ca and (**B**) W, S, Ca, and K in metasomatically altered diorite. Note decrease in Ca concentration and increase of K concentration within main alteration selvage (boundaries marked by white dashed lines) and increasing towards vein with Ca-rich margins (red dashed lines). The distribution of Ca and K is consistent with the remobilization of K during the potassic alteration of wall rocks due to interaction with a mineralized fluid. Red boxes show the location of grains in Figure 8A,F.

Table 1. Total measured scheelite (Sch) and ilmenite (Ilm) in samples.

Sample	Host Rock Type	Scale (Pixels/μm^2)	Area (μm^2)	Total Sch Area (μm^2)	% Sch by Area	WO$_3$ % (% Sch × 0.8)	Total Ilm Area (μm^2) *	% Ilm by Area	Ilm/Sch
SB0830-240.6m	gabbro	1.379	11,266,947	46,259	0.41	0.33	7841	0.07	0.17
SB0834A-118.6	gabbro	0.985	11,953,933	141	0.001	0.001	-	-	-
SB0834A-84.6m	gabbro	0.788	38,557,124	295,668	0.77	0.61	2153	0.01	0.01
SB0845-80.4m	mafic tuff	1.379	15,411,563	54,301	0.35	0.28	3260	0.02	0.06
SB0917-67.7m	felsic tuff	2.956	3,128,848	42,692	1.36	1.09	-	-	-
SB0812-12.8mA	diabase	1.379	8,716,779	31,519	0.36	0.29	-	-	-
SB0812-12.8mB	diabase	1.379	7,568,149	12,013	0.16	0.13	-	-	-
SB0812-12.8mC	diabase	1.379	3,614,850	2558	0.07	0.06	-	-	-

* Ilmenite was not measured in some samples due to its rarity.
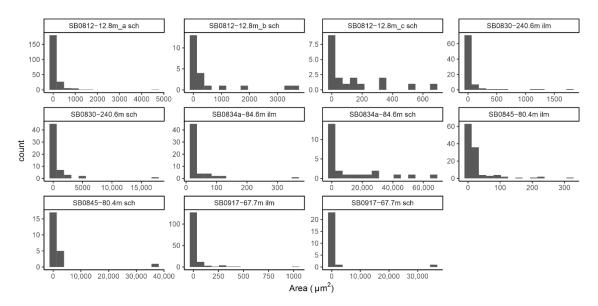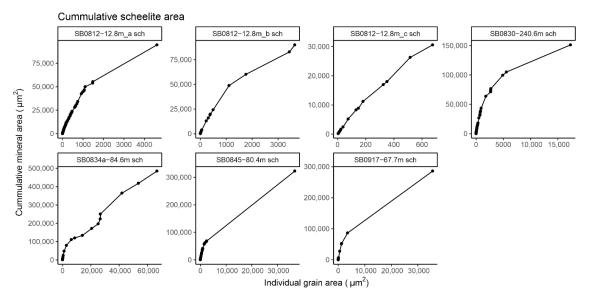
Figure 6. Histograms depicting populations of scheelite (sch) and ilmenite (ilm) grains for five samples.
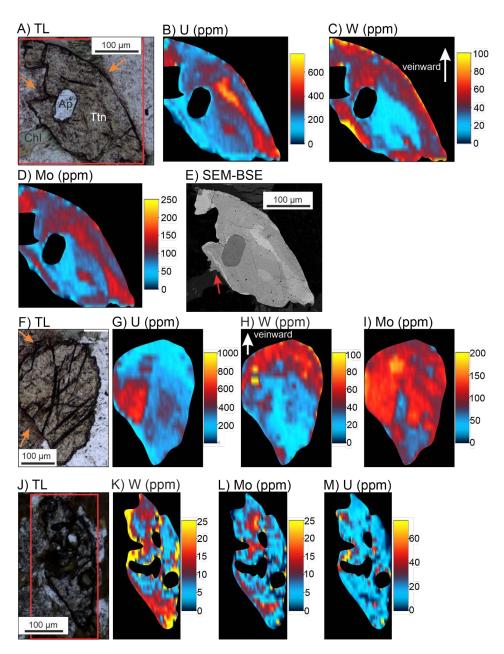

Figure 7. Cumulative grain area of scheelite in measured samples. Note that larger grain size fractions account for the bulk of the mineralization area.
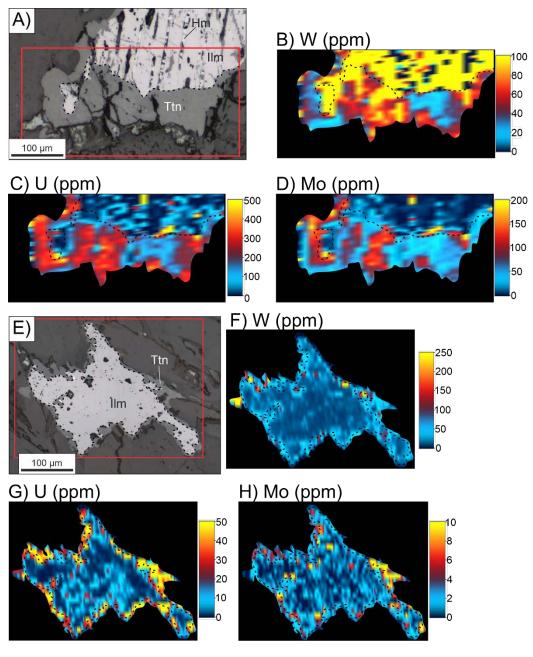
Analysis of the grain size distribution of scheelite using SEM-BSE indicates that micro-inclusions of scheelite in ilmenite are relatively uncommon; however, where present, scheelite inclusions completely encapsulated within ilmenite are commonly less than 2 μm in diameter, although grains as large as 20×10 μm have been observed. Disseminated scheelite grains in vein selvages and the wall rock are typically on the order of 10 μm and grains hosted within quartz veins can be up to 1 cm in diameter, though most large scheelite grains observed are on the order of 0.5 cm. Due to the scarcity and small size of scheelite inclusions, the inclusion of scheelite in ilmenite is not likely to pose any serious concerns regarding W recoveries.

4.4. Mineral Element Maps

Maps for W, U, and Mo are presented in Figures 8 and 9, since W and Mo are of primary economic interest at Sisson Brook and U is important for assessing the suitability for U-Pb dating. Patterns for Rare Earth Elements (REE) enrichment generally correspond to Mo.

Figure 8. Petrographic images and LA ICP-MS maps of titanite showing visible textures and distribution of W, U, and Mo. Maps of magmatic titanite grains (**A–I**) demonstrate enrichment of W and Mo on the veinward side of the grain (top, indicated by white arrow). Elemental abundances are standardized to titanite and other minerals have been masked out in compositional maps. (**A**) Transmitted light image of magmatic titanite (Ttn) grain from diorite with apatite (Ap) inclusion and chlorite (Chl). Red box indicates area of LA ICP-MS mapping, and orange arrows indicate metamictization of surrounding minerals from U in the titanite (sample from drill core SB0806 at 69 m), (**B**) laser ablation map of U, (**C**) laser ablation map of W, (**D**) laser ablation map of Mo. (**E**) SEM-BSE image of grain in A showing coupled dissolution reprecipitation of titanite (red arrow). (**F**) Transmitted light image of magmatic titanite grain from diorite, and orange arrows indicate metamictization of surrounding minerals from U in the titanite (sample from drill core SB0806 at 69 m), (**G**) laser ablation map of U, (**H**) laser ablation map of W, (**I**) laser ablation map of Mo. (**J**) Transmitted light image of metamorphic titanite grain from mafic tuff. Red box indicates area of LA ICP-MS mapping (sample from drill core SB0845 at 57.3 m), (**K**) laser ablation map of W, (**L**) laser ablation map of Mo, (**M**) laser ablation map of U.

Figure 9. Petrographic images of LA ICP-MS maps of magmatic ilmenite mantled with titanite showing textures and elemental distributions of W, U, and Mo. Maps are not calibrated to single mineral and values are qualitative to allow comparison among various mineral phases. Minerals other than titanite and ilmenite have been masked, and the dotted line indicates the titanite-ilmenite interface. (**A**) Reflected light image showing titanite (Ttn) overgrowing ilmenite (Ilm) with hematite exsolution lamellae (Hm). Sample from granodiorite. Red box indicates area of LA ICP-MS mapping (sample from drill core SB0806 at 69 m), (**B**) laser ablation map of W, (**C**) laser ablation map of U, (**D**) laser ablation map of Mo. (**E**) Reflected light image of ilmenite (Ilm) mantled by titanite (Ttn) in gabbro. Red box indicates area of LA ICP-MS mapping (sample from drill core SB0834a at 84.6 m), (**F**) laser ablation map of W, (**G**) laser ablation map of U, (**H**) laser ablation map of Mo.

Three grains of magmatic titanite were mapped from a single thin section of diorite (SB0806-69 m). Optical images of two of these grains are shown in Figure 8A,F. Fracturing is present in the analyzed grains and likely the result of regional tectonic stresses combined with metamictization due to high U contents. Metamict zones can be seen adjacent to the grains in transmitted light (Figure 8A,F) and high

U values (>200 ppm) are measured in the grains examined (Figure 8B,G). Tungsten zoning is evident in magmatic titanite grains and is concentrated along grain boundaries and fractures (Figure 8C,H), and W can be enriched up to 60–80 ppm, where unmodified domains are closer to 20 ppm. Molybdenum concentrations show enrichment patterns similar to that of U along fractures (Figure 8D,I), and enriched domains contain values of approximately 150 ppm Mo compared to 50 ppm in unaltered portions. Tungsten enrichment at the top of the grains in Figure 8C,H occurs on the veinward side of the grains and does not correspond with fracturing. The boundary of these W-rich domain likely represents the edge of a W-mineralizing reaction front at some stage of deposit formation. Tungsten enrichment in Figure 8H corresponds with a decrease in U concentration (Figure 8G), and this correlation may be due to W and U occupying the same site in the titanite lattice or may be due to the nature of the mineralizing fluids. Figure 8E is a SEM-BSE image of the grain in Figure 8A and shows higher molecular density (brighter) areas coincident with measured elevated heavy element concentrations, including as U and Mo. Coupled dissolution reprecipitation (DRP) textures are also evident in Figure 8E, indicating that magmatic titanite was partially remobilized and/or altered during the various mineralizing episodes. This is consistent with micro-XRF mapping of this slide (Figure 5), where both magmatic titanites fall within the envelope of K-metasomatism where Ca is observed to be remobilized.

One mapped titanite grain, hosted in a mafic tuff, is interpreted to be metamorphic in origin. The grain is intergrown with biotite and contains biotite inclusions (Figure 8J). The grain shows slight W and Mo enrichment around its edges (Figure 8K,L), though concentrations are lower relative to magmatic titanite. The grain shows extremely low U levels when compared to those measured in magmatic titanite (Figure 8M). Lower U can be explained by lower abundances in the host mafic tuff versus diorite-hosted grains.

Three examples of metasomatic titanite that overgrew and/or replaced magmatic ilmenite from diorite and gabbro were examined and mapped and two representative grains are presented here (Figure 9). The grain in Figure 9A–D is from diorite, and the grain in Figure 9E–H is from gabbro. Relationships between the titanite and ilmenite are not uniform and indicate that the different episodes of mineralization acted on the formation of the titanite rims. Grains in diorite (e.g., Figure 9A–D) show enrichment of W in the ilmenite relative to the titanite, which is unexpected given the elevated W concentrations measured in altered magmatic titanite. The titanite rims in all measured grains are enriched in U and Mo, though concentrations are much lower than those seen in magmatic titanite. The metasomatic titanites are somewhat similar to the metamorphic titanite (Figure 8J–M), although the metamorphic titanite has much lower maximum W contents. The titanite in Figure 9A–D shows zoning of W, Mo, and U, which may be representative of several episodes of Ti mobilization in the system during successive mineralization events. The ilmenite grain in Figure 9E–H shows very little internal variation, except for an area of elevated U that corresponds with fewer pits in reflected light. This area of higher U is interpreted to represent a less altered core. The texture and the absence of hematite exsolution lamellae in this ilmenite grain indicate that it has been altered and at least partially remobilized.
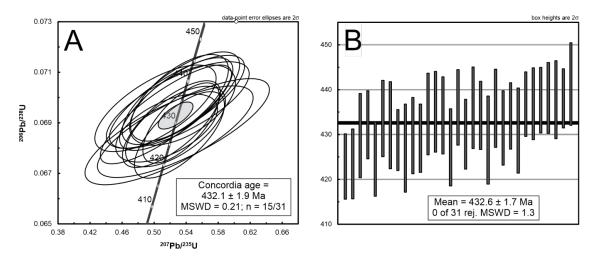
Titanite mantling ilmenite grains shows compositional patterns that are more irregular than the alteration patterns seen in magmatic titanite. Metasomatic titanite contains both high and low concentrations of incompatible elements relative to their included ilmenite. Metasomatic titanite grains also show zoning related to evolving fluid conditions during the formation of the deposit, or to multiple discrete mineralizing pulses/events. The two types of metasomatic titanite observed, i.e., W, Mo, and U enriched and depleted, may reflect formation during separate events and preserve evidence of distinct fluids. The relatively low abundance of W, Mo, and U in the metamorphic titanite compared to the magmatic titanite in the diorite is easily explained by the low abundance of these elements in the mafic tuff and different temperatures of formation of the minerals resulting in different solid solution behavior.

4.5. Whole Rock Geochemistry

Twenty samples were analyzed with a combination of INAA, ICP-MS, and ICP-OES techniques (See Table S1). Spearman correlation coefficients were calculated for each pair of elements. Spearman correlation is a non-parametric measure and preferable to Pearson correlation as it does not require linear correlation as is the case for Pearson correlation [44]. In general, most elements are poorly correlated and with one another (Spearman correlation < 0.95). Calcium correlates moderately well with Ti (Spearman correlation = 0.72), consistent with the occurrence of titanite in most of the rock types observed; however, no elements analyzed correlate strongly with W or Mo in the samples analyzed. These preliminary geochemical results indicate that although petrographic observations indicate that Ca and Ti are locally important to the distribution of scheelite versus wolframite, bulk Ca and Ti concentrations do not appear to have a significant influence on W grade in the samples analyzed.

4.6. U-Pb Geochronology

The Howard Peak Granodiorite sample SB0806-63.7 m was chosen for U-Pb geochronology due to the abundance of large unaltered magmatic titanite crystals in the polished thin section; this intrusion hosts many of the mineralized veins and had yet to be dated. The [204]Pb-corrected concordia age for a subset of concordant titanite from the diorite-granodiorite is 432.1 ± 1.9 Ma (*n* = 15/31; MSWD of 0.21) with a weighted mean [206]Pb/[238]U age of 432.6 ± 1.7 Ma (*n* = 31; MSWD = 1.3) (Figure 10; Table 2; Supplementary Table S2). The U-Pb titanite age of 432 ± 2 Ma is interpreted to represent the crystallization age. The age is 10 Ma years older than the 419.2 and 422.2 U-Pb zircon ages from the Nashwaak Granite [19]. The typical closure temperature of titanite is 650–700 °C [9], which is higher than the maximum temperature of mineralization of 430 °C at Sisson Brook [22]. Only minimal alteration of the titanites is evident near grain boundaries, and any Pb-loss is likely fluid-mediated and related to deformation during the Acadian Orogeny at temperatures below the closure temperature of titanite.

Figure 10. (**A**) U-Pb concordia diagram for titanite from a single thin section of Howard Peak Granodiorite-diorite. Age was determined from 15 points (Table 2; sample from drill core SB0806 at 63.7 m). (**B**) Plot of weighted mean of [206]Pb/[238]U ages for the titanite grains analyzed.

Table 2. Laser ablation data from the analysis of titanite in sample from drill core SB0806 at 63.7 m.

Comments	Used for Age Calculation	U (ppm) *	Th (ppm) *	$\frac{^{207}Pb}{^{235}U}$	2σ	$\frac{^{206}Pb}{^{238}U}$	2σ	$\frac{^{206}Pb}{^{238}U}$ Age	2σ
63.7 m_ttn3c	-	273	538	0.514	0.057	0.0678	0.0012	422.9	7.3
63.7 m_ttn2r	-	281	612	0.452	0.052	0.0679	0.0013	423.5	7.8
63.7 m_ttn8r-2	-	226	726	0.460	0.059	0.0689	0.0015	429.8	9.4
63.7 m_tt5c	-	277	652	0.479	0.056	0.0694	0.0013	432.2	7.6
63.7 m_ttn1r	-	261	729	0.499	0.060	0.0681	0.0014	424.6	8.3
63.7 m_ttn6r-5	yes	334	935	0.502	0.062	0.0696	0.0014	433.6	8.5
63.7 m_ttn4r-3	yes	233	605	0.515	0.067	0.0693	0.0016	432.1	9.7
63.7 m_ttn5r-2	yes	292	1049	0.516	0.052	0.0688	0.0011	428.8	6.8
63.7 m_ttn4r	yes	164	437	0.519	0.086	0.0685	0.0016	427.0	9.8
63.7 m_ttn6r-3	yes	362	913	0.522	0.050	0.0690	0.0014	429.8	8.5
63.7 m_ttn2c	yes	284	742	0.527	0.051	0.0689	0.0013	429.2	7.6
63.7 m_ttn3r	yes	248	686	0.528	0.058	0.0697	0.0015	434.6	9.1
63.7 m_ttn4c	yes	249	884	0.529	0.069	0.0698	0.0015	435.1	9.0
63.7 m_ttn5r	yes	240	623	0.530	0.073	0.0697	0.0014	434.3	8.6
63.7 m_ttn6c	yes	342	834	0.532	0.046	0.0685	0.0014	427.2	8.6
63.7 mttn1c	yes	295	836	0.532	0.050	0.0700	0.0014	436.1	8.4
63.7 m_ttn11r	yes	392	843	0.534	0.039	0.0690	0.0013	430.1	7.8
63.7 m_ttn9r-2	yes	261	722	0.534	0.060	0.0700	0.0015	436.0	9.1
63.7 m_ttn7r	yes	256	800	0.536	0.054	0.0697	0.0013	434.3	7.6
63.6 m_ttn6r	yes	189	525	0.537	0.088	0.0688	0.0016	428.8	9.8
63.7 m_ttn8c	-	206	438	0.539	0.068	0.0700	0.0015	435.9	8.7
63.7 m_ttn6r-2	-	313	1193	0.540	0.052	0.0692	0.0014	431.5	8.3
63.7 m_ttn10c	-	257	555	0.569	0.051	0.0697	0.0012	434.2	7.4
63.7 m_ttn8r-1	-	202	426	0.604	0.070	0.0691	0.0016	430.9	9.5
63.7 m_ttn11r-2	-	274	680	0.532	0.049	0.0701	0.0012	436.8	7.2
63.7 m_ttn4r-2	-	306	886	0.540	0.049	0.0701	0.0013	436.9	8.0
63.7 m_ttn11r-3	-	251	593	0.533	0.056	0.0703	0.0012	437.7	7.3
63.7 m_ttn9r	-	342	853	0.541	0.046	0.0703	0.0013	438.2	7.9
63.7 m_ttn6r-4	-	274	534	0.534	0.054	0.0703	0.0014	437.8	8.7
63.7 m_ttn7c	-	325	707	0.598	0.052	0.0703	0.0011	438.1	6.6
63.7 m_ttn7r-3	-	253	569	0.542	0.055	0.0709	0.0015	441.3	9.2

* U and Th concentrations are semi-quantitative.

5. Discussion

5.1. Compositional Zoning Resulting from Mineralization

Compositional mapping of ilmenite and titanite using LA ICP-MS demonstrates the alteration of titaniferous phases occurred during multiple events by distinct and variable hydrothermal fluids. Protracted hydrothermal systems have been documented in the same metallogenic belt as the Sisson Brook deposit, as recent geochronological studies at the Lake George deposit indicate different magmatic-hydrothermal events responsible for mineralization occurred over a period of approximately 10 Myr [45]. Magmatic titanite shows complex zoning coincident with fractures, i.e., fluid pathways in the grains. It is also possible that some of the zoning in magmatic grains is primary having originated during formation of the grain. Enrichment in most lithophile elements, including U, W, Mo, and REEs, occurs in altered areas, indicating that alteration was caused by evolved fluids that were likely also responsible for mineralization. Fluids interacting with the wall rock along the reaction front likely permeated through the host rock through a combination of microfractures generated by hydrofracturing and possible enhanced porosity by hydrolysis reactions removing silica as early fluids were silica undersaturated [22]. Although evidence of alteration focused along fractures within individual grains is observed in the magmatic titanites, additional work is required to fully understand the fluid transport processes involved. Zoning in magmatic titanite grains with enrichments of only ~60 ppm W and ~100 ppm Mo indicate interaction with mineralizing fluids. Tungsten and Mo are likely substituting in the Ti site of titanite due to the similarities in their ionic radii [5].

The inclusion of scheelite within ilmenite grains that are in turn mantled by metasomatic titanite provides further evidence of the interaction between titaniferous phases and W mineralization, demonstrating that titaniferous phases were at least partially remobilized during the formation of the

deposit. Alteration of magmatic titanite grains by mineralizing fluids has also been demonstrated in other settings, such as at the Ruanjiawan W-Cu-Mo skarn deposit in China [46]. The zoning within titanite overgrowths on ilmenite is variable and preserves evidence of mobilization by both barren and mineralizing fluids. Alteration of metamorphic and metasomatic titanites by stages of infiltrating fluid may be hindered or helped depending on the presence of fractures along and within grain boundaries. The resultant W and Mo enrichment in magmatic and metasomatic titanite from interaction with W-rich fluids is further evidence that titanite is a viable indicator mineral for W-bearing systems [1,5].

5.2. Scheelite Versus Wolframite Saturation

Saturation of scheelite relative to wolframite is controlled by several different factors. As proposed by Nast and Williams-Jones [22], destabilization of KWO_4^- complexes by the removal of K^+ ions occurred due to biotitization and sericitization of amphibole and plagioclase and resulted in the deposition of W mineralization at Sisson Brook. Liberated Ca^{2+} ions from biotitization and sericitization of the gabbro and granodiorite are consumed during the formation of scheelite. Lower Ca abundances in the tuff and clastic sedimentary units accounts for the presence of wolframite over scheelite during some stages of mineralization. The transition from wolframite to scheelite deposition can be explained by three processes: (1) increasing Ca activities in the mineralizing fluids, (2) decreasing aFe, and/or (3) by increasing temperatures in a pro-grading evolving system, since scheelite is stable at higher fluid temperatures than wolframite (see [47]). Inclusions of scheelite within metasomatic ilmenite demonstrates that scheelite and ilmenite were cogenetic during at least one mineralizing phase, where metasomatic ilmenite encapsulated small scheelite grains during growth, and prevented the scheelite grains from getting larger. Biotite, pyrite, and ilmenite formation likely sequestered enough Fe to lower the relative aFe/aCa thereby favouring both scheelite saturation over wolframite and titanite saturation over ilmenite. This evolution of the mineralizing system towards lower relative aFe/aCa with time was noted by Nast [21] and Nast and Williams-Jones [22] who attributed the process to changing fluid-rock ratios during the ore-forming event. The influence of ilmenite formation may also play an important role in an evolving aFe/aCa as ilmenite ($FeTiO_3$) sequesters Fe (and Mn) in the host rocks that would otherwise contribute to the formation of wolframite [$(Fe,Mn)WO_4$] [48].

Multistage formation of W-mineralization (wolframite) from discrete hydrothermal episodes has been documented at the La Bosse stockwork in the Echassieres District of the Massif Central, France [49,50]. The Sisson Brook deposit may represent a similar case given the protracted magmatic and hydrothermal activity present in the area (ca. 432 Ma Howard Peak Granodiorite, ca. 422 to 419 Ma Nashwaak Granite [19], ca. 376 Ma Re-Os molybdenite [7], and ca. 365 Ma late porphyry dykes [25]), but with the evolution of aFe/aCa resulting in episodes of wolframite followed by scheelite mineralization, rather than successive wolframite mineralizing events as is observed at the La Bosse stockwork [49]. Additional geochronological work on metasomatic phases is required to determine the timescales on which W mineralization was formed, and trace element geochemistry of mineralization could discriminate different mineralizing events [49].

Given that Fe is a major constituent of ilmenite, Ti activities in the wall rocks can influence the occurrence and distribution of W phases. Titaniferous phases are more common in gabbro and diorite at Sisson Brook, which is consistent with the observed distribution of scheelite and wolframite as Ti generally shows low mobility in hydrothermal systems [51]. Scheelite deposition in preference to wolframite can be also be the result of an increase in sulfur fugacity after the early stages of mineralization that is associated with the saturation of molybdenite as noted by Nast and Williams-Jones [22]. Increases in sulfur fugacity destabilizes wolframite in favour of tungstenite (WS_2), pyrite, and pyrrhotite [47] and elevated aCa due to potassic alteration will result in the formation of scheelite over tungstenite. Increasing sulfur fugacity would also likely result in the destabilization of ilmenite in favour of hydrothermal phases, such as pyrite and titanite, due to changing redox and/or sulfidation conditions. The formation of later pyrite and titanite following the replacement of ilmenite can be explained by the chloritization of biotite to release additional Ti into the system [51–53].

Proposed general metasomatic reactions are presented in general Equations (1) and (2) below. Equation (1) accounts for the formation of scheelite and ilmenite, whereas Equation (2) accounts for the later formation of titanite from ilmenite. Titanium in Equation (1) may also be derived from hornblende, as SEM-EDS measurements identified TiO_2 concentrations on the order of 1–2 wt% in hornblende.

$$\text{Hornblende } [Ca_2(Fe,Mg,Al)_5(Si,Al)_8O_2(OH)_2] + \text{Plagioclase } [(Na,Ca)(Si,Al)_4O_8] + Ti(OH)_4 + HKWO_4 \rightarrow$$
$$\text{Biotite } [K(Fe,Mg)_3AlSi_3O_{10}(OH)_2] + \text{Scheelite } [CaWO_4] + \text{Ilmenite } [FeTiO_3] \tag{1}$$

$$\text{Biotite } [K(Fe,Mg)_3AlSi_3O_{10}(OH)_2] + \text{Ilmenite } [FeTiO_3] + Ca(OH)_2 + H_2S \rightarrow$$
$$\text{Titanite } [CaTiSiO_5] + \text{Pyrite } [Fe_2S] + \text{Chlorite } [(Mg,Al,Fe)_3(Si,Al)_4O_{10}(OH)_2 \cdot (Mg,Al,Fe)_3(OH)_6] + K(OH) \tag{2}$$

Titaniferous phases can exert controls on W mineralization beyond those determined by Nast and Williams-Jones [22] at the Sisson Brook deposit. Areas with higher Ti concentrations are expected to contain more scheelite than wolframite due to the influence of ilmenite formation on Fe activities. Likewise, biotitization reactions that consume amphibole will increase both Ca and Ti activities in the system, causing preferential saturation of scheelite.

6. Conclusions

1. Compositional mapping at various scales (micro-XRF and LA ICP-MS) demonstrates that both magmatic and metasomatic titanite grains can, in the case of Sisson Brook, record signatures of mineralizing fluids. Magmatic titanite grains examined show inhomogeneous enrichment of both W and Mo with the highest enrichments occurring on the veinward side of the grain, and metasomatic titanites record both mineralized and non-mineralized fluids.
2. The distribution of titaniferous phases in host rocks influences the distribution of W mineralization phases by exerting controls on Fe and Ca activities. Although petrologic observations indicate Ti and Ca phases are important for the distribution of W mineralization phases (i.e., scheelite and wolframite), preliminary bulk Ca and Ti concentrations do not appear to correlate with W, and therefore do not influence the grade of W mineralization based on the samples examined.
3. Unaltered domains of magmatic titanite returned a U-Pb age of 432.1 ± 1.9 Ma for the Howard Peak Granodiorite. This age is approximately 10 Myr older than that of the Nashwaak Granite (419.2 ± 1.8 and 422.2 ± 1.7 Ma; U-Pb zircon [19]) and 54 Myr older than the age of molybdenite mineralization (378.5 ± 1.7 and 376.5 ± 1.6 Ma; Re-Os model ages [7]), indicating that the Sisson Brook area has undergone protracted magmatic and hydrothermal activity. Dating of the metasomatic titanite rims surrounding ilmenite and other metasomatic U-bearing phases could be done to refine the timing of W relative to Mo mineralization.

References

1. Linnen, R.; Che, X. Evaluation of titanite as an indicator mineral for tungsten-skarn mineralization. In *Yukon Exploration Geology 2009*; MacFarlane, K.E., Weston, L.H., Blackburn, L.R., Eds.; Yukon Geological Survey: Whitehorse, YT, Canada, 2010; pp. 223–228.

2. Li, J.D.; Li, X.F.; Xiao, R. In situ LA-ICP-MS U-Pb geochronology and trace element analysis of hydrothermal titanite from the Jiepai W-Cu deposit, South China: Implications for W mineralization. *Can. Mineral.* **2020**, *58*, 45–69. [CrossRef]

3. Horie, K.; Hidaka, H.; Gauthier-Lafaye, F. Elemental distribution in apatite, titanite and zircon during hydrothermal alteration: Durability of immobilization mineral phases for actinides. *Phys. Chem. Earth Parts A/B/C* **2008**, *33*, 962–968. [CrossRef]

4. Xie, L.; Wang, R.-C.; Chen, J.; Zhu, J.-C. Mineralogical evidence for magmatic and hydrothermal processes in the Qitianling oxidized tin-bearing granite (Hunan, South China): EMP and (MC)-LA-ICPMS investigations of three types of titanite. *Chem. Geol.* **2010**, *276*, 53–68. [CrossRef]

5. Che, X.D.; Linnen, R.L.; Wang, R.C.; Groat, L.A.; Brand, A.A. Distribution of trace and rare earth elements in titanite from tungsten and molybdenum deposits in Yukon and British Columbia, Canada. *Can. Mineral.* **2013**, *51*, 415–438. [CrossRef]

6. Frost, B.R.; Chamberlain, K.R.; Schumacher, J.C. Sphene (titanite): Phase relations and role as a geochronometer. *Chem. Geol.* **2001**, *172*, 131–148. [CrossRef]

7. Zhang, W. Petrological and Metallogenic Studies of the Nashwaak Granite and Felsic Dykes Associated with the Sisson Book W-Mo-(Cu) Deposit, West-Central New Brunswick, Canada. Ph.D. Thesis, University of New Brunswick, Fredericton, NB, Canada, 2015.

8. Carocci, E.; Marignac, C.; Cathelineau, M.; Truche, L.; Lecomte, A.; Pinto, F. Rutile from Panasqueira (Central Portugal): An excellent pathfinder for wolframite deposition. *Minerals* **2019**, *9*, 9. [CrossRef]

9. Sun, J.; Yang, J.; Wu, F.; Xie, L.; Yang, Y.; Liu, Z.; Li, X. In situ U-Pb dating of titanite by LA-ICPMS. *Chin. Sci. Bull.* **2012**, *57*, 2506–2516. [CrossRef]

10. Fu, Y.; Sun, X.; Zhou, H.; Lin, H.; Yang, T. In-situ LA–ICP–MS U–Pb geochronology and trace elements analysis of polygenetic titanite from the giant Beiya gold–polymetallic deposit in Yunnan Province, Southwest China. *Ore Geol. Rev.* **2016**, *77*, 43–56. [CrossRef]

11. Bineli Betsi, T.; Lentz, D.R.; Mcfarlane, C. The Nucleus deposit: Superposed Au–Ag–Bi–Cu mineralization systems at Freegold Mountain, Yukon, Canada. *Resour. Geol.* **2016**, *66*, 419–454. [CrossRef]

12. Sinclair, W.D. Porphyry deposits. In *Mineral Deposits of Canada: A Synthesis of Major Deposit Types, District Metallogeny, the Evolution of Geological Provinces and Exploration Methods*; Special Publication, no. 5; Goodfellow, W.D., Ed.; Geological Association of Canada, Mineral Deposits Division: St. John's, NL, Canada, 2007; pp. 223–243.

13. Kirkham, R.V.; Sinclair, W.D. Porphyry copper, gold, molybdenum, tungsten, tin, silver. In *Geology of Canadian Mineral Deposit Types*; Geology of Canada, no. 8; Eckstrand, O.R., Sinclair, W.D., Thorpe, R.I., Eds.; Geological Survey of Canada: Ottawa, ON, Canada, 1996; pp. 421–446.

14. Sinclair, W.D. Vein-stockwork tin, tungsten. In *Geology of Canadian Mineral Deposit Types*; Geology of Canada, no. 8; Eckstrand, O.R., Sinclair, W.D., Thorpe, R.I., Eds.; Geological Survey of Canada: Ottawa, ON, Canada, 1996; pp. 409–420.

15. Ruitenberg, A.A.; Fyffe, L.R. *Characteristics and Tectonic Settings of Granitoid-Related Mineral Deposits in New Brunswick*; Mineral Resources, Geoscience Report 91-1; New Brunswick Department of Natural Resources and Energy: Fredericton, NB, Canada, 1991.

16. Brown, T.; Pitfield, P. Tungsten. In *Critical Metals Handbook*; John Wiley & Sons: Hoboken, NJ, USA, 2014; pp. 385–413.

17. Stewart, H.J.; McLeod, M.J.; Thorne, K.G. *Tungsten*; Mineral Commodity Profile No 7; New Brunswick Department of Natural Resources, Lands, Minerals, and Petroleum Division: Fredericton, NB, Canada, 2011.

18. Zhang, W.; Lentz, D.R.; Thorne, K.G.; McFarlane, C. Geochemical characteristics of biotite from felsic intrusive rocks around the Sisson Brook W–Mo–Cu deposit, west-central New Brunswick: An indicator of halogen and oxygen fugacity of magmatic systems. *Ore Geol. Rev.* **2016**, *77*, 82–96. [CrossRef]

19. Zhang, W.; Lentz, D.R.; Thorne, K.G.; Massawe, R.J.R. Late Silurian-Early Devonian slab break-off beneath the Canadian Appalachians: Insights from the Nashwaak Granite, west-central New Brunswick, Canada. *Lithos* **2020**, *358*, 105393. [CrossRef]

20. Rennie, D.W. *Technical Report on the Sisson Project, New Brunswick, Canada*; Prepared for Northcliff Resources Ltd.: Vancouver, BC, Canada, 2012; p. 161.

21. Nast, H.J. The Geology and Petrochemistry of the Sisson Brook W-Cu-Mo Deposit, New Brunswick. Master's Thesis, McGill University, Montreal, QC, Canada, 1985.

22. Nast, H.J.; Williams-Jones, A.E. The role of water-rock interaction and fluid evolution in forming the porphyry-related Sisson Brook W-Cu-Mo deposit, New Brunswick. *Econ. Geol.* **1991**, *86*, 302–317. [CrossRef]

23. Zhang, W.; Lentz, D.R.; Thorne, K.G. Petrogenesis of the Nashwaak Granite, West-Central New Brunswick, Canada: Evidence from Trace Elements, O and Hf Isotopes of Zircon, and O Isotopes of Quartz. *Minerals* **2020**, *10*, 614. [CrossRef]

24. Bustard, A.L.; Zhang, W.; McFarlane, C.R.M.; Lentz, D.R. Tungsten mineralization processes at the Sisson Brook W-Mo-Cu deposit, Central New Brunswick: The role of formation of titaniferous phases at reaction fronts. *Acta Geol. Sin. Engl. Ed.* **2013**, *87*, 672–675. [CrossRef]

25. Fyffe, L.R.; Thorne, K.G.; Dunning, G.R.; Martin, D.A. U-Pb geochronology of the Sisson Brook Granite Porphyry, York County, west-central New Brunswick. In *Geological Investigations in New Brunswick for 2007*; Minerals, Policy and Planning Division; Martin, G.L., Ed.; New Brunswick Department of Natural Resources: Fredericton, NB, Canada, 2007; pp. 35–54.

26. Whalen, J.B.; Fyffe, L.R.; Longstaffe, F.J.; Jenner, G.A. The position and nature of the Gander–Avalon boundary, southern New Brunswick, based on geochemical and isotopic data from granitoid rocks. *Can. J. Earth Sci.* **1996**, *33*, 129–139. [CrossRef]

27. Fyffe, L.; Johnson, S.; van Staal, C. A review of Proterozoic to Early Paleozoic lithotectonic terranes in the northeastern Appalachian orogen of New Brunswick, Canada, and their tectonic evolution during Penobscot, Taconic, Salinic, and Acadian orogenesis. *Atl. Geol.* **2011**, *47*, 211–248. [CrossRef]

28. Tharalson, E.R.; Monecke, T.; Reynolds, T.J.; Zeeck, L.; Pfaff, K.; Kelly, N.M. The distribution of precious metals in high-grade banded quartz veins from low-sulfidation epithermal deposits: Constraints from μXRF mapping. *Minerals* **2019**, *9*, 740. [CrossRef]

29. Flude, S.; Haschke, M.; Storey, M.; Harvey, J. Application of benchtop micro-XRF to geological materials. *Mineral. Mag.* **2017**, *81*, 923–948. [CrossRef]

30. Schindelin, J.; Arganda-Carreras, I.; Frise, E.; Kaynig, V.; Longair, M.; Pietzsch, T.; Preibisch, S.; Rueden, C.; Saalfeld, S.; Schmid, B. Fiji: An open-source platform for biological-image analysis. *Nat. Methods* **2012**, *9*, 676–682. [CrossRef]

31. Preibisch, S.; Saalfeld, S.; Tomancak, P. Globally optimal stitching of tiled 3D microscopic image acquisitions. *Bioinformatics* **2009**, *25*, 1463–1465. [CrossRef]

32. Petruk, W. Image analysis of minerals. In *Short Course on Image Analysis Applied to Mineral and Earth Sciences*; Petruk, W., Ed.; Mineralogical Association of Canada: Quebec City, QC, Canada, 1989; pp. 6–18.

33. Ulrich, T.; Kamber, B.S.; Jugo, P.J.; Tinkham, D.K. Imaging element-distribution patterns in minerals by laser ablation-inductively coupled plasma-mass spectronomy (LA–ICP–MS). *Can. Mineral.* **2009**, *47*, 1001–1012. [CrossRef]

34. Jenner, F.E.; Arevalo, R.D., Jr. Major and trace element analysis of natural and experimental igneous systems using LA–ICP–MS. *Elements* **2016**, *12*, 311–316. [CrossRef]

35. Paton, C.; Hellstrom, J.; Paul, B.; Woodhead, J.; Hergt, J. Iolite: Freeware for the visualisation and processing of mass spectrometric data. *J. Anal. At. Spectrom.* **2011**, *26*, 2508–2518. [CrossRef]

36. McFarlane, C.R.M.; Luo, Y. U-Pb Geochronology Using 193 nm Excimer LA-ICP-MS Optimized for In-Situ Accessory Mineral Dating in Thin Sections. *Geosci. Can.* **2012**, *39*, 158–172.

37. Faye, G.H.; Sutarno, R. Certified compositional reference materials for the earth sciences. *Can. Mineral.* **1976**, *14*, 164–171.

38. Harley, S.L.; Kelly, N.M. Zircon tiny but timely. *Elements* **2007**, *3*, 13–18. [CrossRef]

39. Rubin, J.N.; Henry, C.D.; Price, J.G. The mobility of zirconium and other "immobile" elements during hydrothermal alteration. *Chem. Geol.* **1993**, *110*, 29–47. [CrossRef]

40. Wang, X.; Chen, J.; Ren, M. Hydrothermal zircon geochronology: Age constraint on Nanling Range tungsten mineralization (Southeast China). *Ore Geol. Rev.* **2016**, *74*, 63–75. [CrossRef]

41. Heaman, L.M. The application of U–Pb geochronology to mafic, ultramafic and alkaline rocks: An evaluation of three mineral standards. *Chem. Geol.* **2009**, *261*, 43–52. [CrossRef]

42. Petrus, J.A.; Kamber, B.S. VizualAge: A novel approach to laser ablation ICP-MS U-Pb geochronology data reduction. *Geostand. Geoanal. Res.* **2012**, *36*, 247–270. [CrossRef]

43. Ludwig, K.R. *Isoplot 3.75: A Geochronological Toolkit for Microsoft Excel*; Special Publication (Vol. 5); Berkeley Geochronology Center: Berkeley, CA, USA, 2012.

44. Reimann, C.; Filzmoser, P.; Garrett, R.; Dutter, R. *Statistical Data Analysis Explained: Applied Environmental Statistics with R*; John Wiley & Sons: Hoboken, NJ, USA, 2011.

45. Lentz, C.; Thorne, K.; McFarlane, C.R.M.; Archibald, D.A. U-Pb, Ar-Ar, and Re-Os geochronological constraints on multiple magmatic–hydrothermal episodes at the Lake George Mine, Central New Brunswick. *Minerals* **2020**, *10*, 566. [CrossRef]

46. Deng, X.-D.; Li, J.-W.; Zhou, M.-F.; Zhao, X.-F.; Yan, D.-R. In-situ LA-ICPMS trace elements and U–Pb analysis of titanite from the Mesozoic Ruanjiawan W–Cu–Mo skarn deposit, Daye district, China. *Ore Geol. Rev.* **2015**, *65*, 990–1004. [CrossRef]

47. Wood, S.A.; Samson, I.M. The hydrothermal geochemistry of tungsten in granitoid environments: I. Relative solubilities of ferberite and scheelite as a function of T, P, pH, and mNaCl. *Econ. Geol.* **2000**, *95*, 143–182. [CrossRef]

48. Lecumberri-Sanchez, P.; Vieira, R.; Heinrich, C.A.; Pinto, F.; Wälle, M. Fluid-rock interaction is decisive for the formation of tungsten deposits. *Geology* **2017**, *45*, 579–582. [CrossRef]

49. Monnier, L.; Salvi, S.; Melleton, J.; Bailly, L.; Béziat, D.; de Parseval, P.; Gouy, S.; Lach, P. Multiple Generations of Wolframite Mineralization in the Echassieres District (Massif Central, France). *Minerals* **2019**, *9*, 637. [CrossRef]

50. Monnier, L.; Salvi, S.; Jourdan, V.; Sall, S.; Bailly, L.; Melleton, J.; Béziat, D. Contrasting fluid behavior during two styles of greisen alteration leading to distinct wolframite mineralizations: The Echassières district (Massif Central, France). *Ore Geol. Rev.* **2020**, *124*, 103648. [CrossRef]

51. Van Baalen, M.R. Titanium mobility in metamorphic systems: A review. *Chem. Geol.* **1993**, *110*, 233–249. [CrossRef]

52. Rice, C.M.; Darke, K.E.; Still, J.W.; Lachowski, E.E. Tungsten-bearing rutile from the Kori Kollo gold mine, Bolivia. *Mineral. Mag.* **1998**, *62*, 421–429. [CrossRef]

53. Yuan, F.; Liu, J.; Carranza, E.J.M.; Zhai, D.; Wang, Y.; Zhang, S.; Sha, Y.; Liu, G.; Wu, J. The Guangshigou uranium deposit, northern Qinling Orogen, China: A product of assimilation-fractional crystallization of pegmatitic magma. *Ore Geol. Rev.* **2018**, *99*, 17–41. [CrossRef]